Low mechanical loss TiO_2-doped GeO_2 coatings for reduced thermal noise in Gravitational Wave Interferometers
Supplemental Material

Gabriele Vajente,[1,*] Le Yang,[2] Aaron Davenport,[3] Mariana Fazio,[3] Alena Ananyeva,[1] Liyuan Zhang,[1] Garilynn Billingsley,[1] Kiran Prasai,[4] Ashot Markosyan,[4] Riccardo Bassiri,[4] Martin M. Fejer,[4] Martin Chicoine,[5] François Schiettekatte,[5] and Carmen S. Menoni[2,3]

[1]*LIGO Laboratory , California Institute of Technology, Pasadena, CA 91125 USA*
[2]*Department of Chemistry, Colorado State University, Fort Collins, CO 80523, USA*
[3]*Department of Electrical and Computer Engineering, Colorado State University, Fort Collins, CO 80523, USA*
[4]*Edward L. Ginzton Laboratory, Stanford University, Stanford, CA 94305, USA*
[5]*Département de Physique, Université de Montréal, Montréal, Québec, Canada*

(Dated: July 28, 2021)

EFFECTIVE MEDIUM APPROACH

The elastic properties of the materials composing the multilayer coatings determine the Brownian noise incurred by the GW detectors where the mirrors are used. Although every single layer can be treated as composed of a homogeneous isotropic material, the layered structure of the stack breaks the symmetry. The multilayer stack cannot be described with simple averages of the single material properties, and the combination of the materials' Young's modulus, Poisson ratio and loss angles that enter in the Brownian noise estimates is different from the combination that determine the decay time of the mode ring-downs in the Gentle Nodal Suspension measurements. Here we briefly describe a unified approach to model both ring-down measurements and Brownian noise, based on an *effective medium* computation [17]. A detailed description of the method and the derivation of all the equations reported here is available in reference [15].

In an isotropic medium, the response to a stress is the same in all direction, and the symmetry implies that it is possible to express the elastic stiffness tensor in terms of only two moduli, for example the Young's modulus Y and Poisson ratio ν or alternatively the bulk and shear moduli K and μ. This is not true for a layered material, but for elastic fields that vary slowly on the scale of the layer thicknesses (other than the discontinuities due to the layers themselves) the elastic properties of the multilayer can be described by an effective medium of lower symmetry, the components of whose stiffness tensor are computed from appropriately weighted averages of combinations of the elastic moduli of the layers [17].

Assuming a structure composed of two different alternating materials with total thicknesses d_A and d_B, we define the average of an elastic quantity as

$$\bar{g} = \langle g \rangle = \frac{d_A}{d_A + d_B} g_A + \frac{d_B}{d_A + d_B} g_B \tag{1}$$

The essence of the effective medium approach is to rearrange the constitutive elastic equations for all layers in forms that do not contain products of quantities that are discontinuous at the boundaries. In that form it is possible to carry out the averaging of equation 1 and write effective constitutive equations for the entire stack. The in-plane strains S_{xx}, S_{yy} and S_{xy} are continuous across the layer boundaries, as are the surface normal stresses T_{zz}, T_{xz} and T_{yx}. Those quantities are the basis of the effective medium averaging. Reference [15] carries out the computations and provides expressions for the elastic stiffness tensor of a layered material in terms of the single material properties. This effective tensor can then be used to compute the elastic response of the film.

When the stack is deposited on a significantly thicker substrate, like the Advanced LIGO+ mirrors or the 1-mm-thick disks used for the ring-down measurements, one can compute the elastic fields in the substrate independently, and use them as boundary conditions for the thin film fields [56]. One can then compute the elastic energy density in the film, using the effective medium stiffness tensor, according to

$$u = \frac{1}{2} \sum_i T_i S_i \tag{2}$$

where the summation is over all six components of the strain and stress tensors given in the Voight notation. We are primarily interested in the power dissipated in the film due to internal friction. This can be computed from the rate at which work is done on an deformed elastic body [55]. For a sinusoidal time dependence of frequency $f = \omega/2\pi$ this is

$$p_{\text{diss}} = -\frac{\omega}{2} \text{Im} \left[\frac{1}{2} \sum_i T_i^* S_i \right] \tag{3}$$

The result depends on the case being considered, since the elastic fields are determined by the substrate. When we compute the Brownian noise, we follow Levin's approach [12], by applying a virtual force F_0 on the front surface of the mirror, distributed like the intensity of

the interferometer Gaussian probe beam, and compute the stress and strain fields for the substrate, as done by Harry et al. in [56]. Ignoring the light penetration into the coating, the Brownian noise is then directly related to the power dissipated by [12]:

$$S(f) = \frac{4k_B T}{\pi f} \frac{p_{\mathrm{diss}}}{2\pi f F_0^2} \tag{4}$$

The power dissipated in the stack when subject to virtual force can be computed using the effective medium stiffness tensor, to obtain the following expression that relates the Brownian noise power spectral density to the elastic properties of the materials composing the layers:

$$\begin{aligned} S(f) = \frac{2k_B T}{\pi^2 f} \frac{d}{w^2} \Bigg\{ & \left[\frac{1}{3} \left\langle \frac{1-2\nu}{(1-\nu)^2} Y \phi_K \right\rangle + \frac{2}{3} \left\langle \frac{1-\nu+\nu^2}{(1-\nu)(1-\nu^2)} Y \phi_\mu \right\rangle \right] \frac{(1+\nu_S)^2 (1-2\nu_S)^2}{Y_S^2} \\ & + \frac{2}{3} \left\langle \frac{(1-2\nu)(1+\nu)}{(1-\nu)^2} (\phi_K - \phi_\mu) \right\rangle \frac{(1+\nu_S)(1-2\nu_S)}{Y_S} \\ & \left[\frac{1}{3} \left\langle \frac{(1+\nu)^2 (1-2\nu)}{(1-\nu)^2} \frac{\phi_K}{Y} \right\rangle + \frac{2}{3} \left\langle \frac{(1+\nu)(1-2\nu)^2}{(1-\nu)^2} \frac{\phi_\mu}{Y} \right\rangle \right] \Bigg\} \end{aligned} \tag{5}$$

It is apparent from this expression that the bulk ϕ_K and shear ϕ_μ loss angles of the materials are averaged in a non-trivial way, that includes both the elastic moduli and their reciprocal. In the limit of equal bulk and shear loss angles, this expression reduces to the simplified form presented in equation 1 of this letter. The results provided by equation 5 have been compared with other models [14, 62] and found to give the same results within a few percents. In the case of the mode ring-downs of the disks used in the Gentle Nodal Suspension, the surface of the disk is stress free but the in-plane shears and dilations are not zero and mode dependent. This difference with respect to the Brownian noise computation hints at the fact that the dissipated power will contain a different combination of the loss angles and elastic moduli. Instead of trying to compute the elastic field in the substrate for each resonant mode analytically, we rely on finite element simulations, performed with COMSOL [66]. The dissipated power in the film (related to the measured Q values) can then be written in terms of the substrate in-plane strains $S_{xx,s}$, $S_{yy,s}$ and $S_{xy,s}$ as follows:

$$p_{\mathrm{diss}} = \frac{\omega}{2} \left\{ \left\langle \frac{Y}{6(1-\nu)^2} \left[2(1-2\nu)\phi_K + (1+\nu)\phi_\mu \right] \right\rangle \left(S_{xx,s} + S_{yy,s} \right)^2 + \left\langle \frac{Y}{2(1+\nu)} \phi_\mu \right\rangle \left[\left(S_{xx,s} - S_{yy,s} \right)^2 + S_{xy,s}^2 \right] \right\} \tag{6}$$

In this case there are no averages involving the reciprocal of the elastic moduli, in contrast to the Brownian noise in equation 5. It is therefore not possible to define an effective loss angle for a multilayer structure that allows simultaneously to describe the power dissipated in the ring-down measurements and the Brownian noise in the coating. For this reason in this letter we use the ring-down measurements for the single layer materials to infer the bulk and shear loss angles, and use those values to compute the Brownian noise for the Advanced LIGO+ mirrors.

In the case of a single isotropic layer on the substrate, all effective medium averages in equation 6 disappear, since there is only one material, and one can show that the power dissipated in the film is proportional to the bulk loss angle multiplied by the bulk energy stored in the film, plus the shear loss angle multiplied by the shear energy stored in the film. This is consistent with the conventional picture that describes the effect of the loss angles in terms of the dilution factors, that are the ratio of the amount of shear or bulk energy in the film divided by the total elastic energy in the resonator [53, 65]. It also allows a simple and computational efficient way to compute the dilution factors from the substrate strains obtained by finite element simulations, which are to very good approximation unchanged by the presence of the thin film, so all that is needed is one finite element simulation of the bare disk with the proper thickness, and then the energies in the film can be computed by straightforward numerical integration of the strains following equation 6. This method allows also to take into account the presence of an annular edge area not covered by the film. It could also allow modeling a non-uniform film.

THIN FILM DEPOSITION AND ANNEALING

For the initial parameter exploration, thin films of TiO_2:GeO_2 with Ti cation concentration of 0%, 27%, and 44%, defined as Ti/(Ti+Ge), were deposited by ion beam sputtering using a biased target deposition system [46], that allowed a convenient tuning of the deposition param-

eters and cation concentration. Mixed TiO_2:GeO_2 thin films of thickness between 200 and 500 nm were deposited on fused silica and silicon substrates for structural and optical characterizations. Homogeneous oxide mixtures were formed by co-sputtering Ge and Ti targets with Ar^+ ions in a reactive oxygen atmosphere. In this process, the selected dopant concentrations were obtained by adjusting the length of the pulses biasing the Ti and Ge targets. In addition, the oxygen partial pressure was adjusted to achieve nearly stoichiometric thin films with high optical quality.

The thin films were also deposited on 75-mm-diameter, 1-mm-thick silica disks, to measure the elastic properties of the material. The un-coated substrates were polished on all surfaces (the two main circular surfaces as well as the barrel) to a standard optical grade, and annealed at 900°C for 10 hours, to obtain high quality factors of the substrate [35, 36], typically in the $0.5-1\times10^8$ range. The 75mm-diameter substrates were held in place in the deposition chamber by a spring-loaded retaining ring, that covered a annular region of 0.5 mm along the entire edge of the sample. This region is therefore not covered by the thin film.

Once the optimal deposition parameters were found, additional films were deposited using a commercial Spector Ion Beam Sputtering system [26]. The deposition of TiO_2:GeO_2 used a metal target, while that of SiO_2 used an oxide target. The process conditions were adjusted to obtain the same optical properties as in the single layers described above.

All films were fully characterized as deposited, and then subjected to heat treatment cycles at various temperatures and of various durations. All annealing cycles were performed in air, by first ramping up the temperature at 100°C per hour, then holding at the target temperature for the desired duration, and finally ramping down at 100°C per hour. When not heated, all samples were stored in vacuum sealed container to avoid water absorption from the atmosphere.

SAMPLE CHARACTERIZATION

The thickness and refractive index of the TiO_2:GeO_2 thin films were obtained from spectroscopic ellipsometry, as shown in figure 1. A Horiba UVISEL ellipsometer was used with an incidence angle of 60°C in the spectral range of 0.59 eV to 6.5 eV. The fitting of ellipsometric data was performed with the DeltaPsi software.

At the laser wavelength of 1064 nm, the transmission of the as-deposited 40-layer structure was 190 ppm and the optical absorption was 46.4 ppm. The absorption loss reduced to 3.1 ppm after annealing at 600C for 10 h.

The structure evolution of the mixture films with annealing was characterized by grazing incidence X-ray diffraction using a Bruker D8 thin film diffractometer operated at an incident angle of 0.5°. The measurement angle

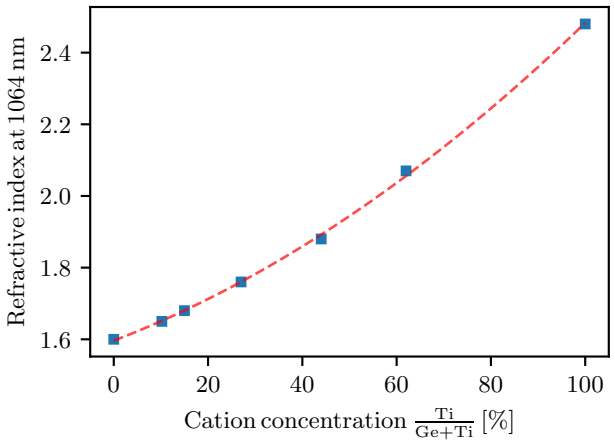

FIG. 1. Measured refractive index of the TiO_2:GeO_2 mixtures, as a function of the Ti cation concentration. The dashed line shows a quadratic fit to the measured data points.

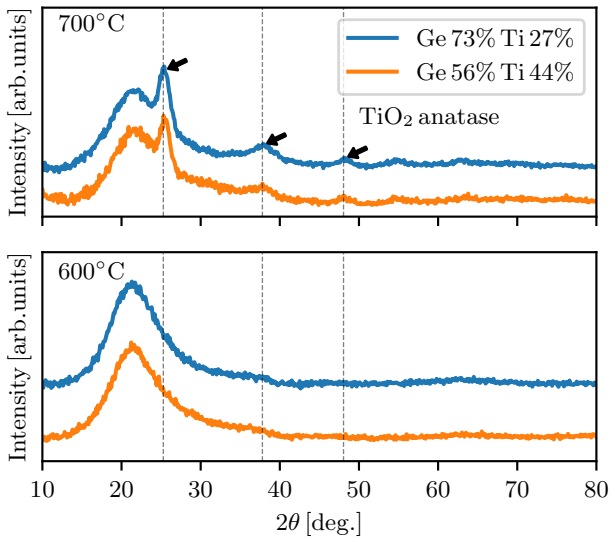

FIG. 2. Grazing incidence x-ray diffractograms from 44% TiO_2:GeO_2 thin films annealed in air at 600°C and 700°C for 10 hours. The broad peak at around 22° corresponds to the fused silica substrate. The peaks at 25.4°, 37.9° and 48.0°, marked with arrows in the figure, are assigned to the TiO_2 anatase crystalline phase (JCPDS 84-1286 [63]).

2θ was varied between 10° and 80°. The results show that all mixture films are amorphous upon annealing at 600°C. Figure 2 shows the spectra of the 27% and 44% TiO_2:GeO_2 thin films annealed at 600°C and 700°C for 10 hours. The thin films are amorphous after 600°C annealing and show incipient crystallization, identified by the peak at 25.3° from crystalline anatase TiO_2 phase [63], when annealed at 700°C. Annealing to 800°C for 10 hours revealed a full crystallization in the 44% mixture

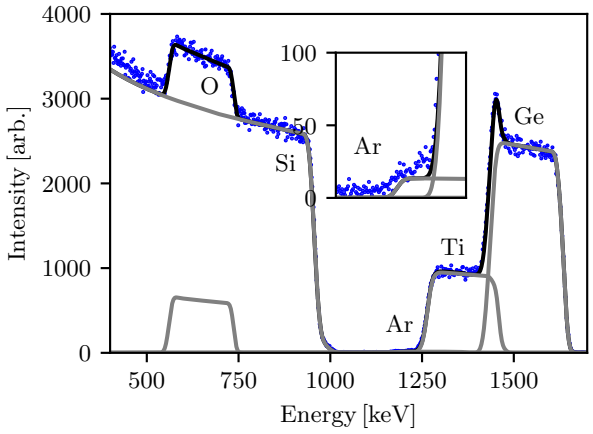

FIG. 3. RBS spectrum (dots) acquired on the sample containing 44% Ti/(Ti+Ge).The spectrum is fitted (black line) with a sum of simulations of single layers containing only the indicated elements. The inset zooms on the region where the lower energy edge of the Ar contribution is visible, between 1150 and 1230 MeV. (It is present at higher energies, but indistinguishable from the large Ti contribution.) A small background signal (5 counts) is visible below 1150 MeV in the inset. It is likely due to multiple scattering but could not be accounted for by the simulation. Since it is also present where the Ar contribution is, the Ar contribution to the spectrum was fitted about 5 counts below the experimental signal. Such background increases non-linearly with decreasing energy and is responsible for a 200 counts discrepancy at 400 keV (left of the main figure) between the experimental spectrum and the simulation.

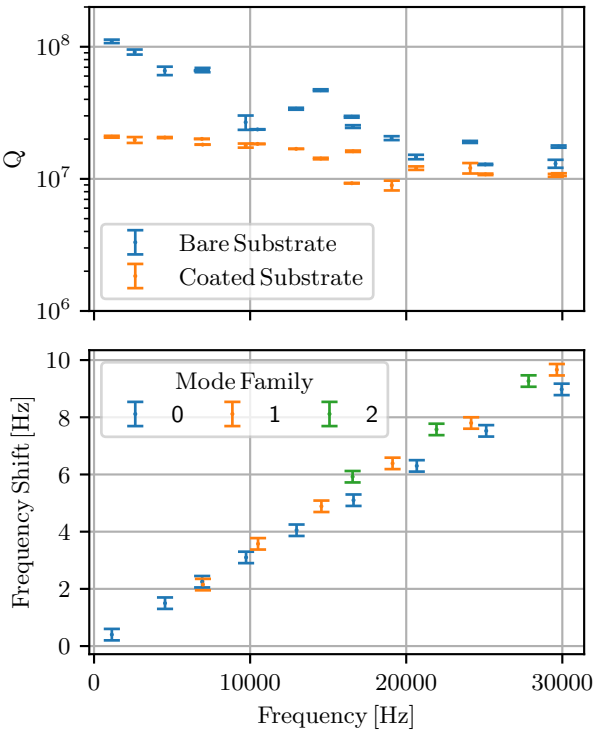

FIG. 4. Example results from the ring-down measurements. The top panel compares the quality factors (Q) of all measured modes, before and after deposition of the 44 % TiO_2:GeO_2 film. The results shown here are for the coated substrate after annealing at 600°C for 108 hours. The bottom panel shows the resonant mode frequency shifts for the same sample, where the different colors correspond to families of modes, enumerated by the number of radial nodes in the oscillation pattern. The uncertainty in the frequency measurement is 0.1 Hz.

film. It was also confirmed that the 44% samples did not show signs of crystallization upon annealing at 600°C for 108 hours.

Rutherford Backscattering spectrometry (RBS) was carried out at the Tandetron accelerator at Université de Montréal. Films deposited on crystalline silicon substrates during the same runs as the main samples were measured using He beams with energies of 2.035 MeV and 3.06 MeV. Prior to these analyses, the spectrum of a sample featuring a few known trace elements at the surface was acquired to determine the detector calibration.

The acquired spectra were then compared to a simulation carried out using SIMNRA [64] to determine each element fraction and the areal atomic density of the layer. Figure 3 shows the spectrum for the sample containing 44% Ti/(Ti+Ge). Within the sensitivity of the technique, all layers are found to be homogeneous, and do not feature a concentration depth profile. The fraction of the detected element in each sample analyzed this way can be found in table I. The Ti and Ge content could be determined with a precision of about 0.5%, while that of oxygen is about 2% because the O peak sits on top of the Si substrate contribution. Given these uncertainties, the samples are found to be stoichiometric. The uncertainty on the areal density is about 3% and is the main contributor to the uncertainty on the mass density, which is ± 100 kg/m^3.

RING-DOWN MEASUREMENTS

The resonant modes of the 75-mm-diameter and 1-mm-thick samples were measured in a Gentle Nodal Suspension [51, 52]. The disks are supported in the center on a spherical silicon surface, and are held in position due to gravity and static friction. This allows for a very low recoil loss at the suspension point and very repeatable measurements for modes with a node at the center of the disk. The frequency f_i and decay time τ_i of about 20 modes are measured multiple times for each sample, before deposition of the thin film, after deposition and after each annealing step. The top panel of figure 4 shows an example of the mode quality factors Q_i, defined as the number of cycles of oscillation that it takes for the mode

Sample	Thickness [nm]	Atomic thickness [$\times 10^{15}$ at/cm^2]	Density [kg/m^3]	Element Concentration O [%]	Ar [%]	Ti [%]	Ge [%]	Ti/(Ti+Ge) [%]
as deposited	480	3297	3370	66.7	0.0	9.4	23.8	28.4
as deposited	321	2325	3720	66.7	0.8	14.6	17.9	44.9
annealed at 600°C	314	2265	3690	67.4	0.3	14.3	18.0	44.3

TABLE I. RBS measurement results for three representative mixed TiO_2:GeO_2 films. The sample in the last row was measured after annealing in air at 600°C. The most notable change is the reduction of the Ar content.

amplitude to be reduced by $1/e$:

$$Q_i = \pi f_i \tau_i \tag{7}$$

From the difference between the Q values measured on the bare disk and on the coated disk, one can compute the excess loss angle due to the film.

$$\delta\phi_i = \frac{1}{Q_i^{\text{coated}}} - (1 - D_i)\frac{1}{Q_i^{\text{bare}}} \tag{8}$$

where D_i is the dilution factor for the i-th mode, defined as the ratio of the elastic energy stored on average in the film divided by the elastic energy stored on average in the entire resonator, film plus substrate. The $\delta\phi_i$ can then be fitted to models of the material loss angles.

The bottom panel of figure 4 shows the shift in the resonant frequency for all modes, due to the additional stiffness and inertia induced by the thin film. By fitting the frequency shifts to finite element models computed with COMSOL, it is possible to estimate the Young's modulus and the Poisson ratio of the film material from the experimental data. The slope of the dependency of the frequency shifts versus frequency is related mostly to the Young's modulus, while the spread along the linear relation is related mostly to the Poisson ratio.

Figure 5 shows the evolution of the loss angle (averaged over all measured modes, and assuming equal bulk and shear angles) and the Young's modulus as a function of the annealing steps. There is a clear increasing trend in the Young's modulus when the film is annealed at higher temperatures, a probable indication of crystallization. The observed trends in mechanical loss and Young's modulus with Ti concentration and annealing are being investigated with atomic structure measurements and modeling.

We note that the analysis of the measurements with different loss angles shows that the TiO_2:GeO_2 shear loss angle is compatible with a constant, frequency independent value. In the resonant modes that are measurable with the Gentle Nodal Suspension, the elastic energy in the film is dominated by shear, with the bulk contribution being typically about a factor 5 smaller. This justifies the approximation of equal and frequency independent loss angles we used in our initial parameter exploration.

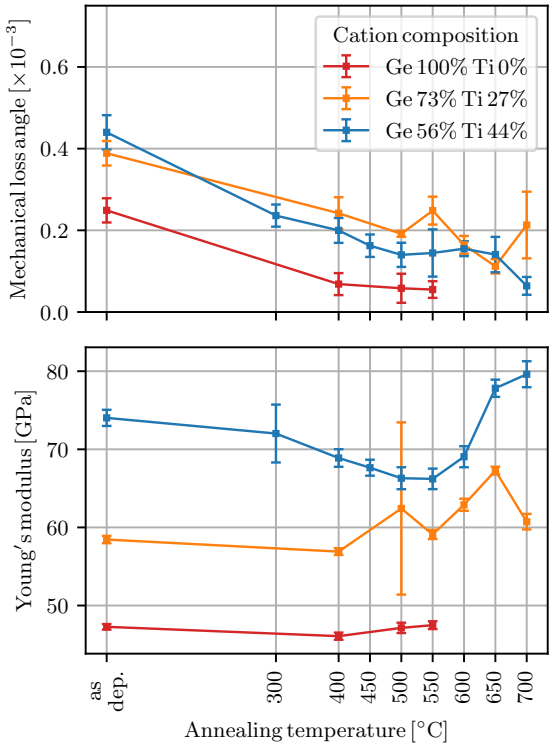

FIG. 5. Measured loss angle (top) and Young's modulus (bottom) of mixed titanium oxide and germanium oxide, for the samples as deposited and after 10-hours-long heat treatments (annealing) in air, at increasing temperatures.

BAYESIAN ANALYSIS OF THE RING-DOWN MEASUREMENTS

For each sample, we measured the resonant frequency shifts δf_i for every mode, and the quality factors $Q_{i,0}$ for the bare disk and the coated substrate $Q_{i,c}$, after annealing. The thickness and density of the films are measured independently with ellipsometry and RBS, as explained above. The material in the single layer is described by its unknown parameters: the Young's modulus Y, the Poisson ratio ν and the frequency dependent bulk and shear loss angles ϕ_K and ϕ_μ. We developed a model of the coated substrate, that can be used to compute the excess loss angle measured in the coated substrate as a function of the material parameters. This model is based on finite element simulations of the bare substrate, per-

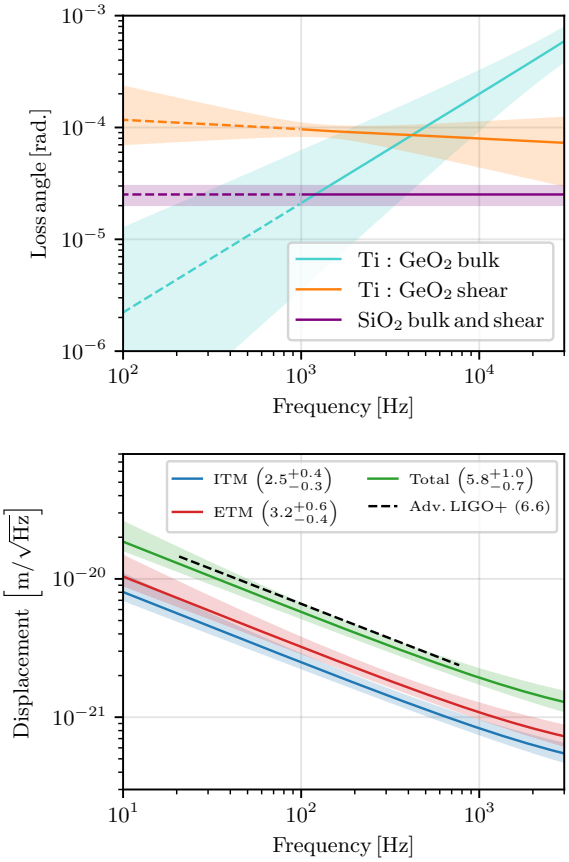

FIG. 6. Top: loss angles corresponding to the model that best predicts the measured data. Bottom: Brownian noise computed with the same model. The numbers in the legend show the predicted Brownian noise at 100 Hz, in units of 10^{-21} m/$\sqrt{\text{Hz}}$.

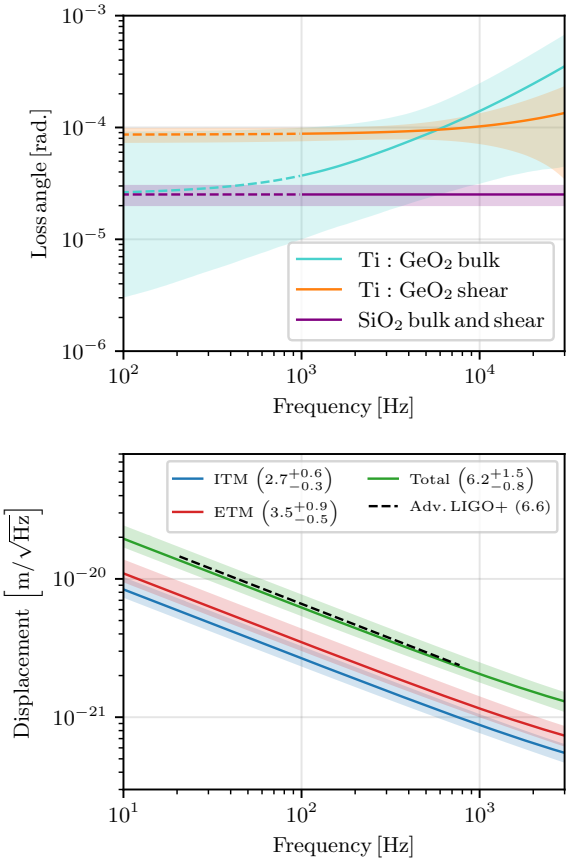

FIG. 7. Top: Loss angles corresponding to the second most probable model that predicts the measured data. Bottom: Brownian noise computed with the same model. The numbers in the legend show the predicted Brownian noise at 100 Hz, in units of 10^{-21} m/$\sqrt{\text{Hz}}$.

formed with COMSOL. The goal of the Bayesian analysis [60] is to compute the posterior probability distribution of the model parameters [Y, ν, $\phi_K(f)$ and $\phi_\mu(f)$] given the measured data (δf_i, $Q_{i,0}$ and $Q_{i,c}$). This can be written using Bayes' theorem:

$$P(Y,\nu,\phi_K,\phi_\mu|\delta f_i,Q_{i,0},Q_{i,c}) \propto P(\delta f_i,Q_{i,0},Q_{i,c}|Y,\nu,\phi_K,\phi_\mu)P(Y,\nu,\phi_K,\phi_\mu)$$

as a function of the data probability given the model parameters $P(\delta f_i,Q_{i,0},Q_{i,c}|Y,\nu,\phi_K,\phi_\mu)$ and the prior probability distribution of the parameters $P(Y,\nu,\phi_K,\phi_\mu)$, which is assumed to be flat within physical ranges. The results are not sensitive to the particular choice of the prior probability, since the data is informative. A Markov chain Monte Carlo (MCMC) algorithm [61] is used to sample the posterior probability.

The loss angles are described with three different models: constant, linearly dependent on frequency, or following a power law:

$$\phi_i = \begin{cases} \phi_{\text{const.}} \\ \phi_{10\,\text{kHz}}\left(1 + m\frac{f-10\,\text{kHz}}{10\,\text{kHz}}\right) \\ \phi_{10\,\text{kHz}}\left(\frac{f}{10\,\text{kHz}}\right)^m \end{cases} \quad (9)$$

Additionally, we either allow for different bulk and shear loss angles, or we force the two angles to be equal. This gives us a total of six models. The sampled posterior probability distribution can be marginalized over all model parameters to obtain the Bayes factor of each of the six model, that is related to the probability of each model given the data. This allows us to determine the model that is favored by the measurements.

The most probable model that describes the internal energy dissipation of the TiO_2:GeO_2 film is a power law frequency dependency, with different bulk and shear loss angles. The power law predicts a steep frequency dependence of the bulk loss angle. The second most probable model is a linear frequency dependency. In the linear

case the slope is constrained to avoid negative loss angle at low frequency. Therefore the linear model cannot describe a frequency dependence as steep as the power law. Nevertheless, both models predict that the bulk loss angle is significantly lower than the shear angle at lower frequencies. The top panels of figure 6 and figure 7 shows the predicted loss angles for both models. The SiO_2 film measurements are best described by equal bulk and shear loss angles, frequency independent, also shown in figures 6 and 7.

The analysis we carried out for the measurements described in this letter is similar to what has been described in reference [53], with two important differences: first, the Young's modulus and Poisson's ratios are modeled together with the loss angles, so the posterior probability distribution of the loss angles takes into account the correlation with the elastic moduli uncertainties; second, the model includes an uncoated edge along the disk border, with a size that can be either be fixed to the measured value, or allowed to vary as part of the Bayesian fit.

The sampled posterior probability distributions of the model parameters can then be used to compute the Brownian noise for a given design of the input and end test mass coatings, using equation 5. Each sample is a set of parameter values, that gives a level of Brownian noise for each frequency. Repeating the computation for all samples in the MCMC output allows us to directly compute the posterior distribution probability of Brownian noise, given the model and the measured data. The bottom panel of figure 6 shows the predicted Brownian noise for the TiO_2:GeO_2 power law model, that is the most probable model given the data. The bottom panel of figure 7 shows the predicted noise for the second most probable model for TiO_2:GeO_2, that is the linear model. In both cases the predicted noise is compatible with the Advanced LIGO+ requirements within the confidence levels.

* vajente@caltech.edu

[1] B. P. Abbott et al. Observation of gravitational waves from a binary black hole merger. *Phys. Rev. Lett.*, 116:061102, Feb 2016.

[2] B. P. Abbott et al. GWTC-1: A Gravitational-Wave Transient Catalog of Compact Binary Mergers Observed by LIGO and Virgo during the First and Second Observing Runs. *Phys. Rev. X*, 9:031040, Sep 2019.

[3] J. Aasi et al. Advanced LIGO. *Class. Quantum Grav.*, 32:074001, 2015.

[4] F. Acernese et al. Advanced Virgo: a second-generation interferometric gravitational wave detector. *Class. Quantum Grav.*, 32(2):024001, 2015.

[5] T. Akutsu et al. KAGRA: 2.5 Generation Interferometric Gravitational Wave Detector. *Nat. Astron.*, 3(1):35–40, 2019.

[6] Gabriele Vajente, Eric K. Gustafson, and David H. Reitze. Chapter Three - Precision interferometry for gravitational wave detection: Current status and future trends. volume 68 of *Advances In Atomic, Molecular, and Optical Physics*, pages 75 – 148. Academic Press, 2019.

[7] J. Steinlechner. Development of mirror coatings for gravitational-wave detectors. *Phil. Trans. Roy. Soc. Lond. A*, 376(2120):20170282, 2018.

[8] D. V. Martynov et al. Sensitivity of the Advanced LIGO detectors at the beginning of gravitational wave astronomy. *Phys. Rev. D*, 93:112004, Jun 2016.

[9] A. Buikema et al. Sensitivity and performance of the Advanced LIGO detectors in the third observing run. *Phys. Rev. D*, 102:062003, Sep 2020.

[10] Alessandra Buonanno and Yanbei Chen. Quantum noise in second generation, signal-recycled laser interferometric gravitational-wave detectors. *Phys. Rev. D*, 64:042006, Jul 2001.

[11] V.B. Braginsky and S.P. Vyatchanin. Thermodynamical fluctuations in optical mirror coatings. *Physics Letters A*, 312(3):244 – 255, 2003.

[12] Yu. Levin. Internal thermal noise in the LIGO test masses: A direct approach. *Phys. Rev. D*, 57:659–663, Jan 1998.

[13] Herbert B. Callen and Richard F. Greene. On a Theorem of Irreversible Thermodynamics. *Phys. Rev.*, 86:702–710, Jun 1952.

[14] Ting Hong, Huan Yang, Eric K. Gustafson, Rana X. Adhikari, and Yanbei Chen. Brownian thermal noise in multilayer coated mirrors. *Phys. Rev. D*, 87:082001, Apr 2013.

[15] M. M. Fejer. Effective Medium Description of Multilayer Coatings. *LIGO Document*, T2100186, 2021.

[16] See supplemental material at [url will be inserted by publisher].

[17] George E. Backus. Long-wave elastic anisotropy produced by horizontal layering. *Journal of Geophysical Research (1896-1977)*, 67(11):4427–4440, 1962.

[18] M Granata, A Amato, L Balzarini, M Canepa, J Degallaix, D Forest, V Dolique, L Mereni, C Michel, L Pinard, B Sassolas, J Teillon, and G Cagnoli. Amorphous optical coatings of present gravitational-wave interferometers. *Classical and Quantum Gravity*, 37(9):095004, apr 2020.

[19] Alex Amato, Silvana Terreni, Vincent Dolique, Danièle Forest, Gianluca Gemme, Massimo Granata, Lorenzo Mereni, Christophe Michel, Laurent Pinard, Benoit Sassolas, Julien Teillon, Gianpietro Cagnoli, and Maurizio Canepa. Optical properties of high-quality oxide coating materials used in gravitational-wave advanced detectors. *Journal of Physics: Materials*, 2(3):035004, jun 2019.

[20] S. Gras and M. Evans. Direct measurement of coating thermal noise in optical resonators. *Phys. Rev. D*, 98:122001, Dec 2018.

[21] A Amato et al. Optical and mechanical properties of ion-beam-sputtered Nb_2O_5 and TiO_2-Nb_2O_5 thin films for gravitational-wave interferometers and an improved measurement of coating thermal noise in Advanced LIGO. *Accepted in Phys. Rev. D*, 2021.

[22] John Miller, Lisa Barsotti, Salvatore Vitale, Peter Fritschel, Matthew Evans, and Daniel Sigg. Prospects for doubling the range of Advanced LIGO. *Phys. Rev. D*, 91:062005, Mar 2015.

[23] The LIGO Scientific Collaboration. Instrument Science White Paper 2020. *LIGO document*, T2000407, 2020.

[24] Xiao Liu, Daniel R. Queen, Thomas H. Metcalf, Julie E. Karel, and Frances Hellman. Hydrogen-Free Amorphous Silicon with No Tunneling States. *Phys. Rev. Lett.*,

113:025503, Jul 2014.

[25] G Vajente, R Birney, A Ananyeva, S Angelova, R Asselin, B Baloukas, R Bassiri, G Billingsley, M M Fejer, D Gibson, L J Godbout, E Gustafson, A Heptonstall, J Hough, S MacFoy, A Markosyan, I W Martin, L Martinu, P G Murray, S Penn, S Roorda, S Rowan, F Schiettekatte, R Shink, C Torrie, D Vine, S Reid, and R X Adhikari. Effect of elevated substrate temperature deposition on the mechanical losses in tantala thin film coatings. *Classical and Quantum Gravity*, 35(7):075001, feb 2018.

[26] Le Yang, Emmett Randel, Gabriele Vajente, Alena Ananyeva, Eric Gustafson, Ashot Markosyan, Riccardo Bassiri, Martin M Fejer, and Carmen S Menoni. Investigation of effects of assisted ion bombardment on mechanical loss of sputtered tantala thin films for gravitational wave interferometers. *Physical Review D*, 100(12):122004, 2019.

[27] Le Yang, Emmett Randel, Gabriele Vajente, Alena Ananyeva, Eric Gustafson, Ashot Markosyan, Riccardo Bassiri, Martin Fejer, and Carmen Menoni. Modifications of ion beam sputtered tantala thin films by secondary argon and oxygen bombardment. *Applied Optics*, 59(5):A150–A154, 2020.

[28] Le Yang, Mariana Fazio, Gabriele Vajente, Alena Ananyeva, GariLynn Billingsley, Ashot Markosyan, Riccardo Bassiri, Martin M Fejer, and Carmen S Menoni. Structural Evolution that Affects the Room-Temperature Internal Friction of Binary Oxide Nanolaminates: Implications for Ultrastable Optical Cavities. *ACS Applied Nano Materials*, 2020.

[29] Mariana A Fazio, Gabriele Vajente, Alena Ananyeva, Ashot Markosyan, Riccardo Bassiri, Martin M Fejer, and Carmen S Menoni. Structure and morphology of low mechanical loss TiO 2-doped Ta 2 O 5. *Optical Materials Express*, 10(7):1687–1703, 2020.

[30] Raffaele Flaminio, Janyce Franc, Christine Michel, Nazario Morgado, Laurent Pinard, and Benoit Sassolas. A study of coating mechanical and optical losses in view of reducing mirror thermal noise in gravitational wave detectors. *Classical and Quantum Gravity*, 27(8):084030, 2010.

[31] M. Abernathy et al. Exploration of co-sputtered Ta_2O_5-ZrO_2 thin films for gravitational-wave detectors. *Submitted to Classical and Quantum Gravity*, 2021.

[32] Alex Amato, Gianpietro Cagnoli, Maurizio Canepa, Elodie Coillet, Jerome Degallaix, Vincent Dolique, Daniele Forest, Massimo Granata, Valérie Martinez, Christophe Michel, Laurent Pinard, Benoit Sassolas, and Julien Teillon. High-Reflection Coatings for Gravitational-Wave Detectors:State of The Art and Future Developments. *Journal of Physics: Conference Series*, 957:012006, feb 2018.

[33] M. Granata, A. Amato, G. Cagnoli, M. Coulon, J. Degallaix, D. Forest, L. Mereni, C. Michel, L. Pinard, B. Sassolas, and J. Teillon. Progress in the measurement and reduction of thermal noise in optical coatings for gravitational-wave detectors. *Appl. Opt.*, 59(5):A229–A235, Feb 2020.

[34] K. Prasai, J. Jiang, A. Mishkin, B. Shyam, S. Angelova, R. Birney, D. A. Drabold, M. Fazio, E. K. Gustafson, G. Harry, S. Hoback, J. Hough, C. Lévesque, I. MacLaren, A. Markosyan, I. W. Martin, C. S. Menoni, P. G. Murray, S. Penn, S. Reid, R. Robie, S. Rowan, F. Schiettekatte, R. Shink, A. Turner, G. Vajente, H-P. Cheng, M. M. Fejer, A. Mehta, and R. Bassiri. High Precision Detection of Change in Intermediate Range Order of Amorphous Zirconia-Doped Tantala Thin Films Due to Annealing. *Phys. Rev. Lett.*, 123:045501, Jul 2019.

[35] Steven D. Penn, Alexander Ageev, Dan Busby, Gregory M. Harry, Andri M. Gretarsson, Kenji Numata, and Phil Willems. Frequency and surface dependence of the mechanical loss in fused silica. *Physics Letters A*, 352(1):3 – 6, 2006.

[36] Alexandr Ageev, Belkis Cabrera Palmer, Antonio De Felice, Steven D Penn, and Peter R Saulson. Very high quality factor measured in annealed fused silica. *Classical and Quantum Gravity*, 21(16):3887–3892, jul 2004.

[37] Sonja Rau, Christian Enss, Siegfried Hunklinger, Peter Neu, and Alois Würger. Acoustic properties of oxide glasses at low temperatures. *Phys. Rev. B*, 52:7179–7194, Sep 1995.

[38] K. A. Topp and David G. Cahill. Elastic properties of several amorphous solids and disordered crystals below 100 K. *Zeitschrift für Physik B Condensed Matter*, 101(2):235–245, Mar 1996.

[39] I W Martin, R Nawrodt, K Craig, C Schwarz, R Bassiri, G Harry, J Hough, S Penn, S Reid, R Robie, and S Rowan. Low temperature mechanical dissipation of an ion-beam sputtered silica film. *Classical and Quantum Gravity*, 31(3):035019, jan 2014.

[40] Le Yang, Gabriele Vajente, Mariana Fazio, Alena Ananyeva, GariLynn Billingsley, Ashot Markosyan, Riccardo Bassiri, Kiran Prasai, Martin M. Fejer, and Carmen S. Menoni. Enhanced Medium Range Order in Vapor Deposited Germania Glasses at Elevated Temperatures. *arXiv preprint arXiv:2102.08526*, 2021.

[41] Wei Jin, Rajiv K. Kalia, Priya Vashishta, and José P. Rino. Structural transformation in densified silica glass: A molecular-dynamics study. *Phys. Rev. B*, 50:118–131, Jul 1994.

[42] Rashid Hamdan, Jonathan P. Trinastic, and H. P. Cheng. Molecular dynamics study of the mechanical loss in amorphous pure and doped silica. *The Journal of Chemical Physics*, 141(5):054501, 2014.

[43] Massimo Granata, Elodie Coillet, Valérie Martinez, Vincent Dolique, Alex Amato, Maurizio Canepa, Jérémie Margueritat, Christine Martinet, Alain Mermet, Christophe Michel, Laurent Pinard, Benoît Sassolas, and Gianpietro Cagnoli. Correlated evolution of structure and mechanical loss of a sputtered silica film. *Phys. Rev. Materials*, 2:053607, May 2018.

[44] Alex Amato, Silvana Terreni, Massimo Granata, Christophe Michel, Benoit Sassolas, Laurent Pinard, Maurizio Canepa, and Gianpietro Cagnoli. Observation of a Correlation Between Internal friction and Urbach Energy in Amorphous Oxides Thin Films. *Scientific Reports*, 10(1):1670, Feb 2020.

[45] Alex Amato, Silvana Terreni, Massimo Granata, Christophe Michel, Laurent Pinard, Gianluca Gemme, Maurizio Canepa, and Gianpietro Cagnoli. Effect of heating treatment and mixture on optical properties of coating materials used in gravitational-wave detectors. *Journal of Vacuum Science & Technology B*, 37(6):062913, 2019.

[46] Zhurin V V et al. Biased target deposition. *Journal of Vacuum Science & Technology A: Vacuum, Surfaces, and Films*, 18(1):37, 2000.

[47] Wei-Kan Chu. *Backscattering Spectrometry, 1st Edition.* Academic Press, 1978.

[48] Alexei Alexandrovski, Martin Fejer, A Markosian, and

Roger Route. Photothermal common-path interferometry (PCI): new developments. In *Solid State Lasers XVIII: Technology and Devices*, volume 7193, page 71930D. International Society for Optics and Photonics, 2009.

[49] Roger P. Netterfield, Mark Gross, Fred N. Baynes, Katie L. Green, Gregory M. Harry, Helena Armandula, Sheila Rowan, Jim Hough, David R. M. Crooks, Martin M. Fejer, Roger Route, and Steven D. Penn. Low mechanical loss coatings for LIGO optics: progress report. In Michael L. Fulton and Jennifer D. T. Kruschwitz, editors, *Advances in Thin-Film Coatings for Optical Applications II*, volume 5870, pages 144 – 152. International Society for Optics and Photonics, SPIE, 2005.

[50] Matthew Robert Abernathy, Xiao Liu, and Thomas H Metcalf. An overview of research into low internal friction optical coatings by the gravitational wave detection community. *Materials Research*, 21, 2018.

[51] E. Cesarini, M. Lorenzini, E. Campagna, F. Martelli, F. Piergiovanni, F. Vetrano, G. Losurdo, and G. Cagnoli. A "gentle" nodal suspension for measurements of the acoustic attenuation in materials. *Review of Scientific Instruments*, 80(5):053904, 2009.

[52] G. Vajente, A. Ananyeva, G. Billingsley, E. Gustafson, A. Heptonstall, E. Sanchez, and C. Torrie. A high throughput instrument to measure mechanical losses in thin film coatings. *Review of Scientific Instruments*, 88(7):073901, 2017.

[53] Gabriele Vajente, Mariana Fazio, Le Yang, Anchal Gupta, Alena Ananyeva, Garilynn Billinsley, and Carmen S. Menoni. Method for the experimental measurement of bulk and shear loss angles in amorphous thin films. *Phys. Rev. D*, 101:042004, Feb 2020.

[54] Tianjun Li, Felipe A. Aguilar Sandoval, Mickael Geitner, Ludovic Bellon, Gianpietro Cagnoli, Jérôme Degallaix, Vincent Dolique, Raffaele Flaminio, Danièle Forest, Massimo Granata, Christophe Michel, Nazario Morgado, and Laurent Pinard. Measurements of mechanical thermal noise and energy dissipation in optical dielectric coatings. *Phys. Rev. D*, 89:092004, May 2014.

[55] L D Landau, L P Pitaevskii, A M Kosevich, and E M Lifshitz. *Theory of Elasticity, 3rd edition*. Elsevier, 1986.

[56] Gregory M Harry, Andri M Gretarsson, Peter R Saulson, Scott E Kittelberger, Steven D Penn, William J Startin, Sheila Rowan, Martin M Fejer, D R M Crooks, Gianpietro Cagnoli, Jim Hough, and Norio Nakagawa. Thermal noise in interferometric gravitational wave detectors due to dielectric optical coatings. *Classical and Quantum Gravity*, 19(5):897–917, feb 2002.

[57] Iain Martin and Stuart Reid. *Coating thermal noise*, page 31–54. Cambridge University Press, 2012.

[58] Massimo Granata, Emeline Saracco, Nazario Morgado, Alix Cajgfinger, Gianpietro Cagnoli, Jérôme Degallaix, Vincent Dolique, Danièle Forest, Janyce Franc, Christophe Michel, Laurent Pinard, and Raffaele Flaminio. Mechanical loss in state-of-the-art amorphous optical coatings. *Phys. Rev. D*, 93:012007, Jan 2016.

[59] Matthew Abernathy, Gregory Harry, Jonathan Newport, Hannah Fair, Maya Kinley-Hanlon, Samuel Hickey, Isaac Jiffar, Andri Gretarsson, Steve Penn, Riccardo Bassiri, Eric Gustafson, Iain Martin, Sheila Rowan, and Jim Hough. Bulk and shear mechanical loss of titania-doped tantala. *Physics Letters A*, 382(33):2282–2288, 2018. Special Issue in memory of Professor V.B. Braginsky.

[60] A Gelman, J B Carlin, H S Stern, D B Dunson, A Vehtari, and D B Rubin. *Bayesian Data Analysis, 3rd edition*. Chapman and Hall, 2013.

[61] Daniel Foreman-Mackey, David W. Hogg, Dustin Lang, and Jonathan Goodman. emcee: The MCMC Hammer. *Publications of the Astronomical Society of the Pacific*, 125(925):306, March 2013.

[62] William Yam, Slawek Gras, and Matthew Evans. Multimaterial coatings with reduced thermal noise. *Phys. Rev. D*, 91:042002, Feb 2015.

[63] Kheamrutai Thamaphat, Pichet Limsuwan, and Boonlaer Ngotawornchai. Phase characterization of TiO2 powder by XRD and TEM. *Agriculture and Natural Resources*, 42(5):357–361, 2008.

[64] Matej Mayer. SIMNRA, a simulation program for the analysis of NRA, RBS and ERDA. *AIP Conference Proceedings*, 475, 1999.

[65] D R M Crooks, P Sneddon, G Cagnoli, J Hough, S Rowan, M M Fejer, E Gustafson, R Route, N Nakagawa, D Coyne, G M Harry, and A M Gretarsson. Excess mechanical loss associated with dielectric mirror coatings on test masses in interferometric gravitational wave detectors. *Classical and Quantum Gravity*, 19(15):4229–4229, jul 2002.

[66] Comsol multiphysics.